Check for updates

Modelling and simulation of four-stage collision energy absorption system based on magneto rheological absorber

**Pavan Kumar Archakam ·
Sreekumar Muthuswamy** [ID]

Abstract The world is moving towards applying intelligent technologies in automobiles, with focus on the development of autonomous vehicles. These vehicles are equipped with devices to predict and avoid dangerous situations such as vehicle crashes, pedestrian hits, etc. Such devices are mostly used in pre-crash management but not during crash. Hence, there is a requirement of smart crash energy absorption system that works during crashes and modulates its energy absorption capability as per the severity of crash. Thus, the proposed methodology involves development of mathematical modelling and dynamic simulation of a four-stage collision energy absorption system. The Dodge Neon vehicle is considered as a base model with 4 DoF lumped parameter modelling (LPM). The proposed model is equipped with four impact absorption elements such as a bumper, magneto rheological absorber (MRA), spring, and a piston-cylinder with shear plate assembly, that are in series. The MRA is an intelligent device which plays a vital role to make a system to be smart or semi-active by adjusting the crash absorbing capability while altering the power distribution to MRA as per the severity of crash. The modified Bouc-Wen model is utilized for MRA, which is non-linear in nature, and the spring-dashpot model has been considered for other elements of the proposed system. Dynamic expressions have been derived and simulated to validate the capability of the proposed model against the existing base model. The proposed model exhibits great capability in terms of displacement, deceleration, and time of crash of the occupant's cabin. The proposed design can also be utilized for the electrical vehicles (EVs) as an add-on system because of the absence of crushable mechanical elements.

Abbreviations

Parameters related to MRA

α, α_a	Evolutionary coefficients, N/m
α_b	Evolutionary coefficient varying linearly with the applied voltage, N V^{-1} m^{-1}
β, γ	Hysteresis parameters of yield elements, m^{-2}
A	Dimensionless quantity controlling the behaviour of the model
c_0	Viscous damping coefficient at high velocities, N s/m

P. K. Archakam · S. Muthuswamy (✉)
Centre for AI, IoT, and Robotics, Department
of Mechanical Engineering, Indian Institute
of Information Technology, Design and Manufacturing,
Kancheepuram, Chennai 600127, India
e-mail: msk@iiitdm.ac.in

🦋 Springer

c_{0a}, c_{1a}	Damping coefficient related to c_0 and c_1, N s/m
c_{0b}, c_{1b}	Damping coefficient related to c_0 and c_1 varying linearly with the applied voltage, N s V^{-1} m^{-1}
c_1	Viscous damping coefficient at low velocities, N s/m
E_{max}	Maximum energy absorbed, J
F_{max}	Maximum damping force, N
F_{MR}	Damping force, N
k_0	Stiffness at high velocities, N/m
k_1	Accumulator stiffness, N/m
n	Exponential parameter that varies between 1 to 2.
V	Voltage applied, V
u	Filtered voltage, V
$\dot{u}$	Derivative of filtered voltage, V/s
η	Coefficient of first order voltage filter, s^{-1}
x_0	Initial displacement of spring k_1, m
x_{rel}	Relative displacement, m
y	Displacement of the piston, m
z	Evolutionary displacement component, m
$\dot{z}$	Evolutionary velocity component, m/s

Parameters related to vehicle

c	Damping constant of bumper, N s/m
c_{1b}, c_{2b}, c_{3b}	Damping elements of frontal parts of the vehicle, N s/m
c_3	Damping constant corresponding to stage-4, N s/m
F_1	Force at stage-1, N
F_3	Force at stage-3, N
F_4	Force at stage-4, N

k	Stiffness of bumper, N/m
k_{1b}, k_{2b}, k_{3b}	Stiffness of frontal parts of the vehicle, N/m
k_2	Conventional spring stiffness for stage-3, N/m
k_3	Stiffness corresponding to stage-4, N/m
M_1	Mass of suspension and lower longitudinal structural members, kg
M_2	Mass of engine, engine cradle, and upper longitudinal structural members, kg
M_3	Mass of fire wall and part of body on its back, kg
M_4	Mass of occupant's cabin, kg
T_{peak}	Time to reach peak entity, s
x_1, x_2, x_3, x_4	Displacement of M_1, M_2, M_3, and M_4, m
$\dot{x}_1, \dot{x}_2, \dot{x}_3, \dot{x}_4$	Velocity of M_1, M_2, M_3, and M_4, m/s
$\ddot{x}_1, \ddot{x}_2, \ddot{x}_3, \ddot{x}_4$	Acceleration of M_1, M_2, M_3, and M_4, m/s^2
V_i	Initial velocity of the vehicle, m/s

1 Introduction

The current scenario of vehicle collisions and increasing number of fatalities on roads due to transformation of high-impact energy into passenger cabin has become serious concern in many countries. A car crash is such a dangerous phenomenon, which causes an extreme intrusion towards the occupant's cabin. There are institutions established with crash test facilities internationally. Also, standards are available for enhancing impact energy absorption capability of vehicles during high-speed collisions. These standards include New Car Assessment Programme, Federal Motor Vehicle Safety Standards 208-occupant crash protection, and Insurance Institute of Highway Safety (Khattab and a 2010). In India, the test centres available as an initiation of National Automotive Testing and R&D Infrastructure Project (NATRIP) are: International Center for Automotive Technology,

Global Automotive Research Center, National Automotive Test Tracks, and Automotive Research Association of India. All these facilities are established particularly for testing and homologation. Such R&D infrastructure facilities developed by the Government of India are for delivering comfortable, safe, and high-performance vehicles to the consumers (http://www.natrip.in/ 2011).

The physics behind the collision of the vehicle can be modelled in numerous ways such as LPM, finite element modelling, multibody dynamic modelling, and hybrid modelling. The destructive crash test of a vehicle is more complex and expensive due to the requirement of costly equipment. Thus, most of the researchers depend on mathematical replica of crash phenomenon by using these methods (Mei and Thole 2008). Amongst the above methods, an LPM technique has been used in the present work due to its closest outputs compared with experimental test results with ease of operation. The usage of bio-inspired materials in the development of crashworthiness structures have been increased in the present days of research. Xiao et.al have proposed six various cross-sectional models of horsetail-bionic thin-walled structures and validated their performance with outcomes of finite element simulation (Xiao et al. 2016).

Furthermore, several technological advancements are available in the form of passive and active systems to provide comfort and safety to passengers. These are either pre-crash or fully crash avoiding technologies as shown in Table 1. In spite of this, there is a need of a semi-active system, which could work when a vehicle encounter a crash. Thus, the proposed system works during crash occurrence and adjusts the damping force to counteract the impact force based on a semi-active device called, MRA. MRA contributes an important role in making the entire structure to be intelligent by adjusting the damping force as per electro magnetization of the coil inside the piston.

The following studies were also observed in the past towards utilization of various elements in absorbing impact energy that originates from high-speed crashes. The stiffness of the longitudinal member, which consists of an extendable hydraulically driven intelligent structure was modified as per the severity of the frontal impact. (Jawad 2002). Whereas, Elmarakbi and Zu (2006) have proposed couple of smart structures, that are fixed and extendable in nature. Also, the authors followed an insightful methodology, called the incremental harmonic balance method, to improve the crashworthiness of front structure while encountering full and offset impacts. Further, energy absorption structures were proposed by means of pneumatic elements (Cao et al. 2012), that are capable of extending or compressing the beam that absorbs energy according to impact. Multiple shock absorbers were attached to the front and back frames of the "Baja vehicle" to reduce the force of impact during the frontal and rear crashes by absorbing the impact energy (Goher et al. 2017). Also, the authors simulated "Baja frame" by transient dynamic analysis in the ANSYS workbench for different contact situations.

The theoretical design of a novel 4-stage collision energy absorbing system, which includes a bumper, MRA, spring, and piston cylinder with shear plate assembly had been proposed in an earlier work (Jain and Sreekumar 2016). Soumitra Singh et al. (Kachhwaha et al. 2020) developed a mathematical model of a vehicle under crash with four DoF system consisting of bumper, engine and engine room, body of the vehicle, and occupants, including passive restraints called seat belt and airbag. The vehicle behaviour was studied in detail in an earlier work by combining MRA in series and parallel modes with one and two DoF models during various impact velocities (Archakam and Muthuswamy 2021).

Table 1 Safety systems to protect from crash	Sl. No	Passive systems	Active-systems
	1	Seat belt	Anti-lock braking system
	2	Air bags	Electronic stability program
	3	Impact attenuators	Traction control system
	4	Bumper and crumple zones	Advanced driver assistance systems, automated driving, pre-crash warning alerts & autonomous emergency braking

The present trend in the design of automobiles is moving toward EVs to counteract the depletion of natural resources and also to completely reduce air pollution. These battery-powered EVs do not have mechanical frontal parts such as, internal combustion engine, engine cradle, radiator, etc. to absorb energy during collision. Instead of mechanical parts, there are battery packs that need to take this energy to reduce the intrusion towards the occupant's cabin. With this as an objective, Hao et al. have proposed flexible battery packs and optimized to get maximum crash energy absorption capability (Hao et al. 2017). But there may be an occurrence of fire in the battery packs which may limit this approach to a certain extent of crash. Hence, the proposed multi-stage collision energy absorption system addresses this issue in EVs by deploying the advanced crash-proof system with MRA as an intelligent member.

The proposed multi stage non-linear dynamic model is intricate, novel, and developed by positioning MRA and other crash absorbing elements inside the frontal structure of the vehicle. The focus is on the development of mathematical model for multi-stage collision energy absorption system for passenger cars based on MRA along with dynamic simulation. The total system with all components is modelled in LPM technique. The parameters like mass, stiffness, damping coefficient have been selected based on structural material properties of the Dodge-Neon vehicle under crash available in (Marzbanrad and Pahlavani 2011). The MRA has been modelled with the help of modified Bouc-Wen model (non-linear hysteresis parametric model) proposed by Spencer et al. (1997). The smart system has been assembled in front overhang of the vehicle by arranging four-stage elements in series, where MRA contributes a significant role in transformation of the system from passive to semi-active. Numerical analysis has been performed to compare the kinematic responses of the base vehicle and the vehicle equipped with the proposed system.

This article is organized as follows. The brief introduction on MRA and proposed methodology are discussed in Sect. 2. Section 3 presents the mathematical modelling and dynamic equations of the existing and proposed models with LPM technique. The critical parameters selection is a major task in the simulation performed numerically, which is also presented in Sect. 3. Section 4 consists of dynamic simulation along with results and discussions. The results are

categorised into crash kinematics and behaviour of the embedded elements of the proposed system along with MRA during the crash for various velocities of the car and also for different voltages supplied to MRA. Finally, conclusions are drawn in Sect. 5, followed by references.

2 Methodology

MR fluid (MRF) is a smart material in the form of liquid capable of altering its viscosity when subjected to a magnetic field. Rabinow invented MRF at the US National Bureau of Standards in the middle of the of twentieth century (Rabinow 1948). It is prepared by mixing magnetizable particles (1-10 μm) 0–40% by volume in the carrier fluid. Frequently used carrier fluids are synthetic oil or mineral oil. In a recent research, the MRF was developed by storing them in a different metal foams and finite element simulations were performed to validate the dynamic response along with experimental results (Liu et al. 2015). Zhi Shen et.al proposed a new MR damper using metal foam with the help of dimensional optimization and experimental study on the mechanical performance was carried out using a self-developed test rig (Zhi Shen et al. 2020). Different types of MR materials, their modelling, and applications had been studied by Ahmed et al. (Ahamed et al. 2018).

The semi-active device, called MRA, resembles a hydraulic damper in appearance but contains MRF in place of hydraulic fluid with an electromagnetic coil around the piston. Also, there is an accumulator to restore the MRF as per requirements. The MR effect has been achieved in a small gap between piston head and cylinder (active region) while moving the piston in an enclosed cylinder, as shown in Fig. 1a. The MR damper works based on the principle of electro magnetization of MRF through an electromagnetic coil present inside the piston to increase or decrease the damping effect based on external disturbance. These particles align themselves simultaneously once the electromagnetic coil is activated with the current / voltage driver and transforms the fluid from liquid to semi-solid and next to solid-state and vice versa, as depicted in Fig. 1b. This nature of fluid restricts the piston movement and thus the damping effect has been achieved.

Fig. 1 MRA. **a** Components of MRA and **b** Operating principle

(a)

(b)
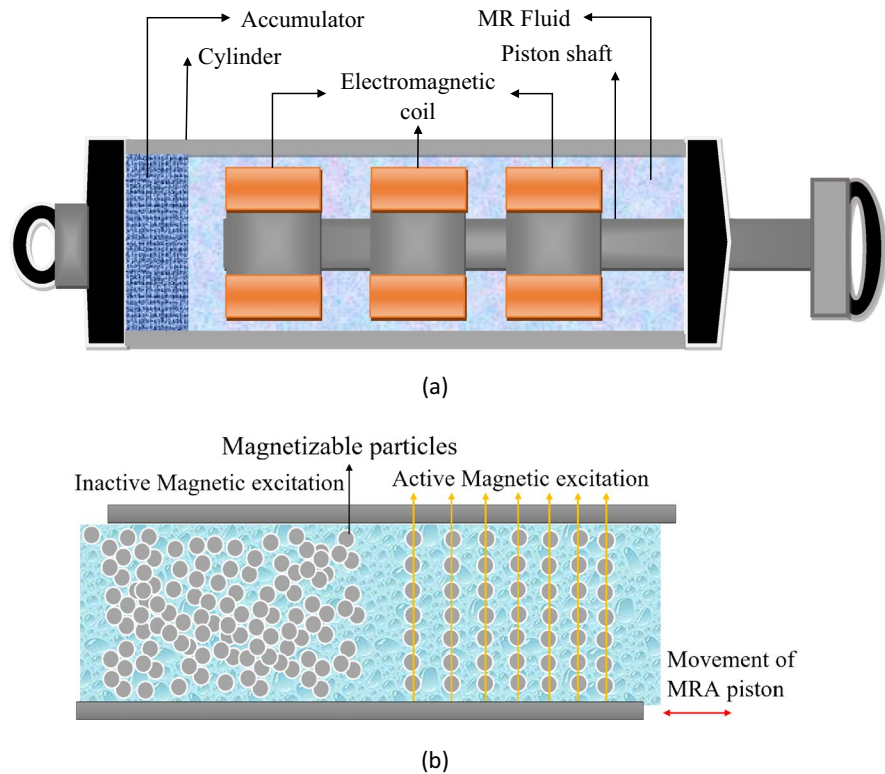
MRAs are utilized in four working modes such as shear mode (structural composites, clutches, breaks, chucking, and locking devices), valve mode (dampers,shock absorbers, servo valves, actuators, and hydraulic controls), squeeze mode (small-amplitude vibration devices and impact dampers), and mixed mode (developed in recent years by achieving two modes at a time) based on the movement of fluid between the plates and based on an application (Zhu et al. 2012).

Structural advancements of MRA are broadly categorized into three aspects such as magnetic circuit, coil number and distribution, and damping channel (Yuan et al. 2019). Additionally, some researchers have also studied applications of MR actuator in multi-DoF systems with focus on design requirements like geometric optimization, principle of working, and control schemes (Oh et al. 2022). The applications of MR technology are versatile such as MR clutches and breaks in automobiles (Pisetskiy and Kermani 2021), bearings (Bompos and Nikolakopoulos 2011), semi-active suspension and torsional devices (Suvarna et al. 2021), devices for mitigating the vibrations during the seismic activity outbreaks

(Spencer et al. 1998), and medical devices (Gao et al. 2019; Liu et al. 2022).

MRA has many input and output variables that are responsible for the actuation behaviour. The input variables are, the voltage supplied to MRA and the corresponding displacement of the associated structure. One of the output variables is the damping force, which is maintained by varying the magnetic flux density around the coil to reduce the effect of impact force. The magnetic flux density changes by varying the voltage supplied to the coil. Thus, the mathematical model includes the coupling effect of magneto-mechanical variables. Most of the researchers concentrated on increasing the magnetic flux density there by achieving enhancement in the damping force. Current trend of research is on the optimization of design variables by using two different approaches, finite element analysis (Krishna et al. 2017) and various optimization techniques such as particle swam optimization, genetic algorithm, etc. (Muthalif et al. 2021).

Various types of models, which are well known for MRA modelling are quasi static, dynamic parametric, dynamic non parametric, dynamic models,

and inverse dynamic models (Rossi et al. 2018). Among the above, the current work requires a dynamic parametric modelling of MRA so as to integrate such dampers in the vehicle. The dynamic parametric models like Gamota and Filisko, Dahl, Lugre, Bingham, Bouc-Wen, and modified Bouc-Wen models, etc. are widely known as mechanical models (Eshkabilov 2016). The modified Bouc-Wen model is considered in the current work because of its better repeatability as evidenced in past research works (Azar et al. 2020; Jiang and Wen 2020) related to several applications as non-linear systems. This model also revealed a closed approximation with physical test results for different input excitations, as proved by Spencer (Spencer et al. 1997).

The proposed methodology for the dynamic modelling of the multi-stage collision energy absorption system is presented in Fig. 2. Initially, the dynamic modelling of the base vehicle with 4 DoF has been done based on LPM. The parameters like mass, stiffness, and damping coefficient have been selected by considering the optimized parameters of crash test

performed on the Dodge-Neon vehicle (Marzbanrad and Pahlavani 2011).

The dynamic expressions of the proposed 4 DoF model equipped with MRA and other elements are obtained first. Further, the proposed multi-stage crash energy absorption model and base model have been compared in terms of crash kinematics such as intrusion (deformation), velocity, and deceleration of passenger's cabin for various high impact velocities. Simultaneously, the behaviour and characteristics of MRA and other energy absorbing elements have also been captured from the proposed model.

3 Mathematical modelling

3.1 Base model of the vehicle

The principle of LPM is to convert any structure/body into lumped masses connected with energy absorbing and dissipating elements such as spring and dashpots respectively. The passenger car can be modelled with several lumped masses and additionally,
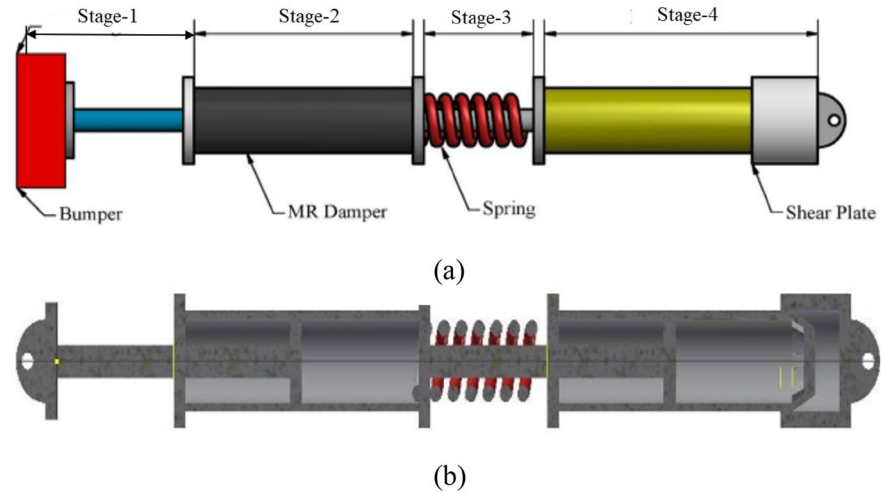

Fig. 2 Methodology of the proposed system
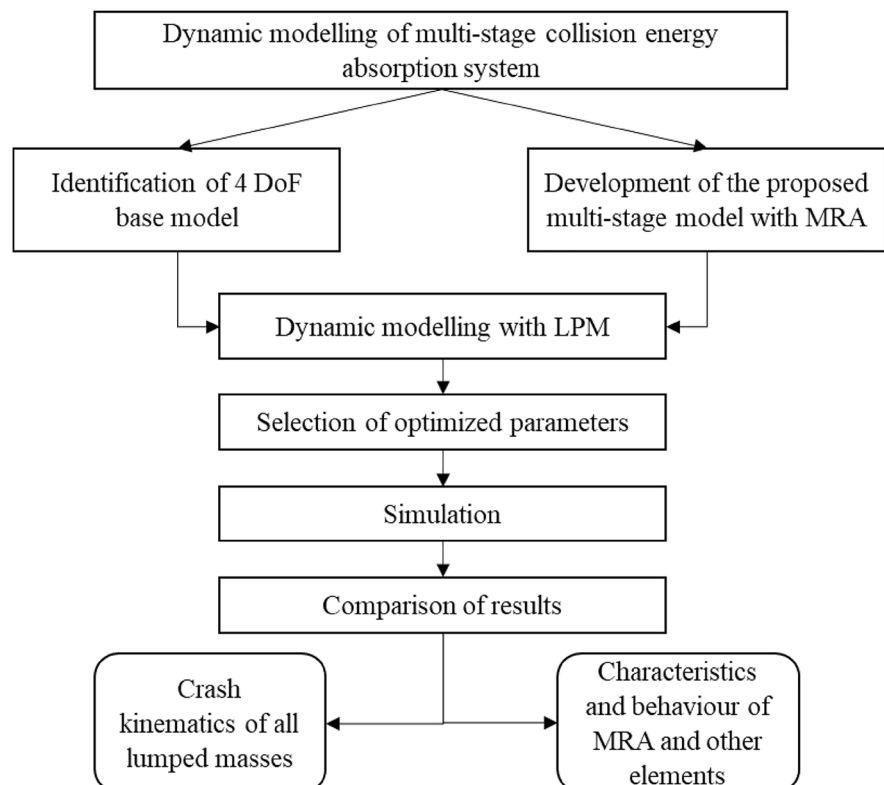
Fig. 3 Four-DoF base model of frontal collision
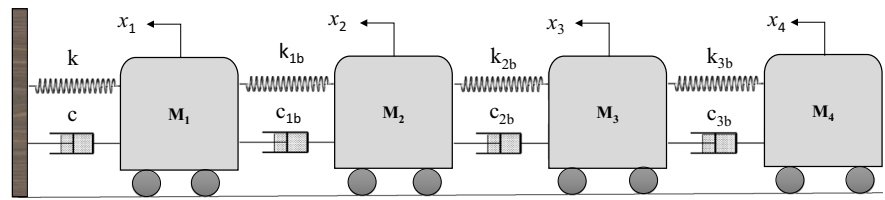
Fig. 4 CAD model of the multi-stage collision energy absorption system, **a** 3D model and **b** Sectional view (Jain and Sreekumar 2016)


(a)

(b)

spring-dashpots are connected in between the lumped masses to exhibit behaviour of structure. Here, the base model consists of 4 DoF as shown in Fig. 3 which is accurate in predicting crash behaviour and hence incorporated in the proposed multi-stage absorption system.

The dynamic equations of the existing four DoF model have been derived based on Newton's second law of motion and are presented below.

$$
\left.\begin{cases}
M_1\ddot{x}_1 + c\dot{x}_1 + c_{1b}(\dot{x}_1 - \dot{x}_2) + kx_1 + k_{1b}(x_1 - x_2) = 0 \\
M_2\ddot{x}_2 + c_{1b}(\dot{x}_2 - \dot{x}_1) + c_{2b}(\dot{x}_2 - \dot{x}_3) + k_{1b}(x_2 - x_1) + k_{2b}(x_2 - x_3) = 0 \\
M_3\ddot{x}_3 + + c_{2b}(\dot{x}_3 - \dot{x}_2) + c_{3b}(\dot{x}_3 - \dot{x}_4) + k_{2b}(x_3 - x_2) + k_{3b}(x_3 - x_4) = 0 \\
M_4\ddot{x}_4 + c_{3b}(\dot{x}_4 - \dot{x}_3) + k_{3b}(x_4 - x_3) = 0
\end{cases}\right\}
$$

(1)

3.2 Proposed multi-DoF model with MRA

The multi-stage collision energy absorption system consists of four energy absorption elements such as bumper, MRA, spring, and shear plate with piston-cylinder assembly as described in an earlier work
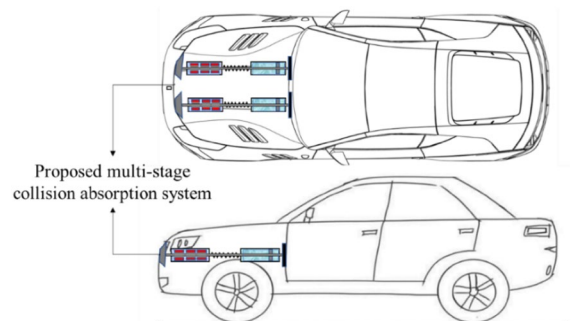
Fig. 5 Integration of proposed multi-stage collision energy absorption system in passenger car

(Jain and Sreekumar 2016) which is shown in Fig. 4. Two of these proposed crash energy absorption systems have been attached in the front end of the passenger car and operates in parallel. One side of them is attached to the bumper end and other ends are with the chassis, as shown in Fig. 5.

The present work totally concentrates on the modelling of a four-DoF system and its dynamic

model so as to capture the behaviour of a vehicle during crash. Spencer model is used for the MRA and classical spring- dashpot model is used to represent other elements of the proposed system. All the above individual elements have been added in series to form a four DoF model, as depicted in Fig. 6.

This system helps in increasing the time of crash and also reduces the impact force on the occupant's cabin. Newton's second law of motion has been used for deriving the dynamic (second-order differential) equations of the proposed model as detailed below.

3.2.1 Masses, M_1 and M_2:

The free body diagrams (FBD) for M_1 and M_2 are presented in Fig. 7a and b respectively. The vehicle is considered to be crashed against a rigid barrier with an initial velocity of V_i, and the same is assumed for all the four masses. The restraints such as spring, damper, and MR actuator are performing their elastic and damping activities in the opposite direction of vehicle movement so as to face the impact.
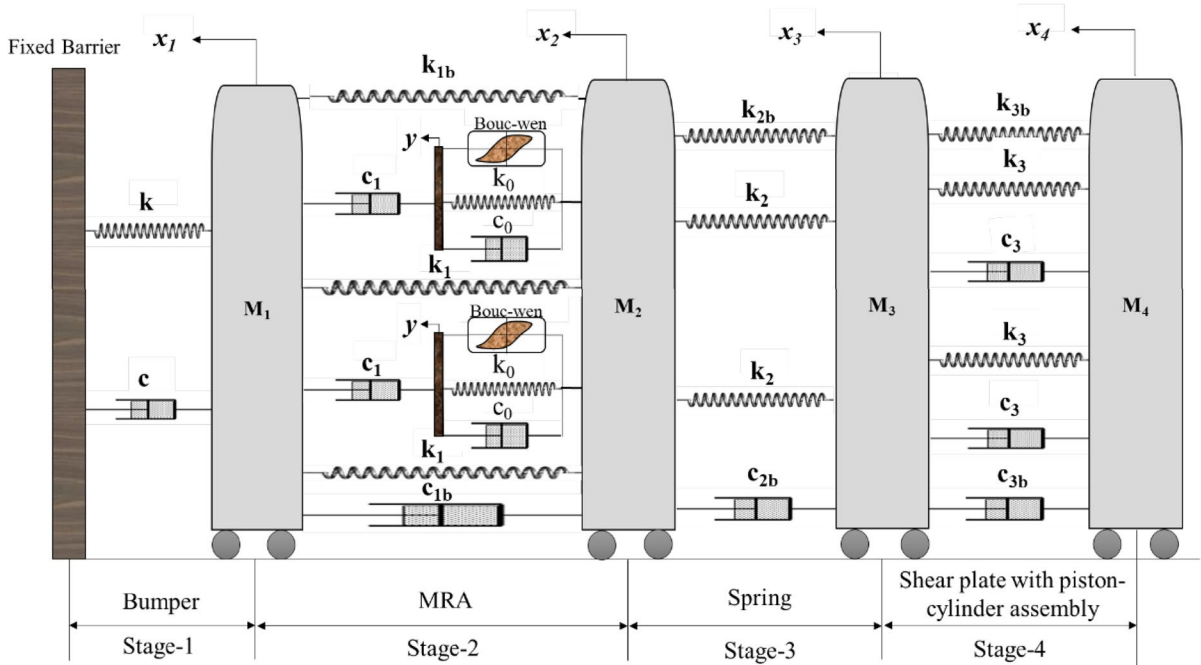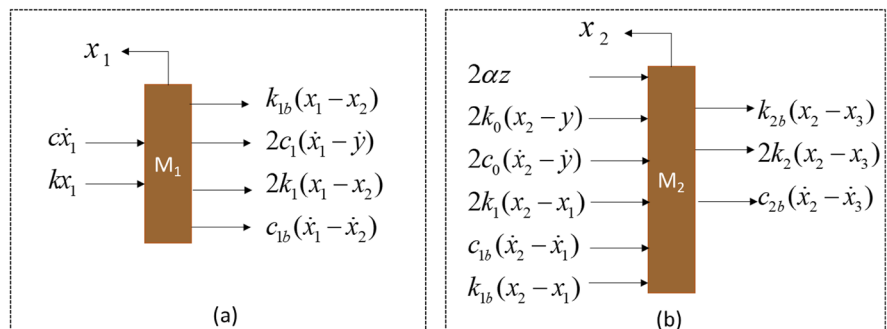
The dynamic equations are as follows

Fig. 6 LPM of the vehicle with proposed multi-stage crash energy absorption system

Fig. 7 FBD for, **a** M_1 and **b** M_2

$$M_1\ddot{x}_1 + c\dot{x}_1 + 2c_1(\dot{x}_1 - \dot{y}) + c_{1b}(\dot{x}_1 - \dot{x}_2)$$
$$+ kx_1 + (2k_1 + k_{1b})(x_1 - x_2) = 0 \qquad (2)$$

$$\left\{\begin{array}{l} M_2\ddot{x}_2 + c_{1b}(\dot{x}_2 - \dot{x}_1) + c_{2b}(\dot{x}_2 - \dot{x}_3) + (2k_2 + k_{2b})(x_2 - x_3) \\ + 2[c_0(\dot{x}_2 - \dot{y}) + k_0(x_2 - y) + \alpha z] + (2k_1 + k_{1b})(x_2 - x_1) \end{array}\right\} = 0$$
$$(3)$$

3.2.2 MRA

The LPM of MRA and its FBDs are depicted in Fig. 8. The governing equations are obtained as under.

Following expressions are derived from Fig. 8b

$$c_1(\dot{y} - \dot{x}_1) + c_0(\dot{y} - \dot{x}_2) + k_0(y - x_2) - \alpha z = 0 \qquad (4)$$

$$c_1(\dot{y} - \dot{x}_1) = \alpha z + c_0(\dot{x}_2 - \dot{y}) + k_0(x_2 - y) \qquad (5)$$

$$\dot{y} = \frac{1}{c_0 + c_1}[\alpha z + c_0\dot{x}_2 + c_1\dot{x}_1 + k_0(x_2 - y)] \qquad (6)$$

Damping force experienced by MRA obtained from Fig. 8c is presented below.

$$F_{MR} = \alpha z + c_0(\dot{x}_2 - \dot{y}) + k_0(x_2 - y) + k_1(x_2 - x_1) \qquad (7)$$

The following expression is obtained by substituting Eq. (5) in Eq. (7)

$$F_{MR} = c_1(\dot{y} - \dot{x}_1) + k_1(x_2 - x_1) \qquad (8)$$

where, $\dot{y}$ can be obtained from Eq. (6).

Modified form of evolutionary velocity component of MRA ($\dot{z}$) for the proposed configuration based on Spencer et al. (1997) is presented below.

$$\dot{z} = -\gamma z|\dot{x}_2 - \dot{y}||z|^{n-1} - \beta(\dot{x}_2 - \dot{y})|z|^n + A(\dot{x}_2 - \dot{y}) \quad (9)$$

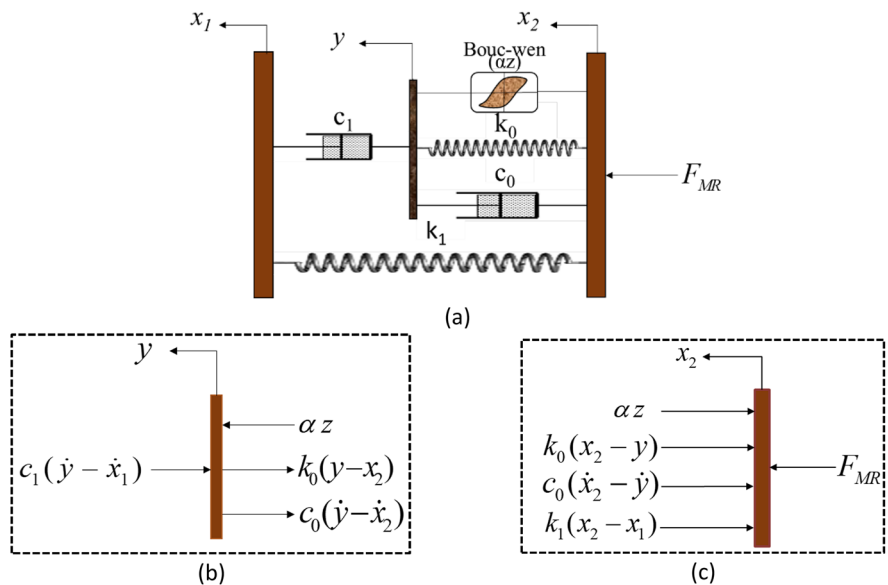Now, the following expression for M_2 is obtained by substituting Eq. (5) in Eq. (3)

$$\left\{\begin{array}{l} M_2\ddot{x}_2 + c_{1b}(\dot{x}_2 - \dot{x}_1) + c_{2b}(\dot{x}_2 - \dot{x}_3) + (2k_2 + k_{2b})(x_2 - x_3) \\ + 2c_1(\dot{y} - \dot{x}_1) + (2k_1 + k_{1b})(x_2 - x_1) \end{array}\right\} = 0$$
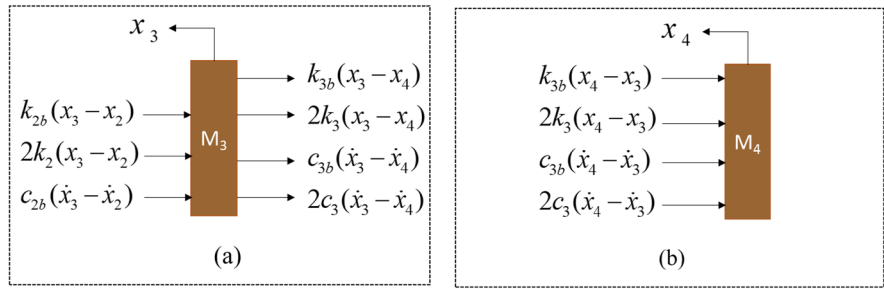$$(10)$$

3.2.3 Similarly, for masses, M_3 and M_4:

The FBD for M_3 and M_4 are depicted in Fig. 9.
The set of dynamic equations are

Fig. 8 Modified Bouc-Wen model of MRA, a LPM of MRA for proposed configuration, b FBD of component y, and c FBD for F_{MR}

Fig. 9 FBD for, **a** M_3 and **b** M_4

(a)

(b)

$$\left.\begin{array}{l} M_3\ddot{x}_3 + c_{2b}(\dot{x}_3 - \dot{x}_2) + (2c_3 + c_{3b})(\dot{x}_3 - \dot{x}_4) \\ + (2k_2 + k_{2b})(x_3 - x_2) + (2k_3 + k_{3b})(x_3 - x_4) \end{array}\right\} = 0$$

(11)

$$M_4\ddot{x}_4 + (2c_3 + c_{3b})(\dot{x}_4 - \dot{x}_3) + (2k_3 + k_{3b})(x_4 - x_3) = 0$$

(12)

Finally, the dynamic equations which would govern the crash kinematics of all individual mass elements of the system are grouped as under.

$$\left.\begin{array}{l} M_1\ddot{x}_1 + c\dot{x}_1 + 2c_1(\dot{x}_1 - \dot{y}) + c_{1b}(\dot{x}_1 - \dot{x}_2) + (2k_1 + k_{1b})(x_1 - x_2) + kx_1 = 0 \\ M_2\ddot{x}_2 + 2c_1(\dot{y} - \dot{x}_1) + c_{1b}(\dot{x}_2 - \dot{x}_1) + c_{2b}(\dot{x}_2 - \dot{x}_3) + (2k_1 + k_{1b})(x_2 - x_1) + (2k_2 + k_{2b})(x_2 - x_3) = 0 \\ M_3\ddot{x}_3 + (2c_3 + c_{3b})(\dot{x}_3 - \dot{x}_4) + c_{2b}(\dot{x}_3 - \dot{x}_2) + (2k_2 + k_{2b})(x_3 - x_2) + (2k_3 + k_{3b})(x_3 - x_4) = 0 \\ M_4\ddot{x}_4 + (2c_3 + c_{3b})(\dot{x}_4 - \dot{x}_3) + (2k_3 + k_{3b})(x_4 - x_3) = 0 \end{array}\right\}$$

(13)

Further, the spencer model of MRA consists of the following four expressions (Spencer et al. 1997), that are governed by the filtered voltage u and applied voltage *V*. the first order filter η in Eq. (17) relates u and V.

$$\alpha = \alpha_a + \alpha_b u$$

(14)

$$c_0 = c_{0a} + c_{0b}u$$

(15)

$$c_1 = c_{1a} + c_{1b}u$$

(16)

$$\dot{u} = -\eta(u - V)$$

(17)

3.3 Selection of parameters

The parameter selection is a very critical part in the dynamic simulation and it is based on the similarities of existing and proposed model, especially the number of DoF of model considered. Thus, both the models are having 4 DoF and the parameters have been selected from the literature (Marzbanrad and Pahlavani 2011). Here, the MRA has been modelled based

Table 2 Parameters considered for MRA @200 kN

Parameter	Value	Parameter	Value
c_{0a}	110,000	k_0	2.0
c_{0b}	114,300	k_1	9.7
c_{1a}	8,359,200	x_0	0
c_{1b}	7,482,900	γ	164.0
α_a	46,200	β	164.0
α_b	41,200	A	1107.2
η	100	n	2.0

Table 3 Parameters considered for 4 DoF base-model (Marzbanrad and Pahlavani 2011)

Parameter	Value	Parameter	Value
M_1	350.00	k_{1b}	1,141,520.38
M_2	220.00	k_{2b}	1,011,727.51
M_3	700.00	k_{3b}	681,806.21
M_4	80.00	c_{1b}	2,480,317.34
k	48,344.98	c_{2b}	8.58
c	20,621.11	c_{3b}	178.40

on the well-known Spencer model, governed by the damping force, as it would reduce the high impact force during crash. Thus, the parameters considered for the present purpose are extracted from 200 kN MR damper (Talatahari et al. 2012) and shown in Table 2. The parameters for the base model were optimized as per the experimental results of the crash test of Dodge Neon vehicle and listed in Table 3. The proposed model can be considered as a (multi-DoF system) free vibration problem with $x_1 = x_2 = x_3 = x_4 = 0$ m, and $\dot{x}_1 = \dot{x}_2 = \dot{x}_3 = \dot{x}_4 = 9.72 - 23.61$ m/s as boundary conditions.

The structural parameters of spring and piston cylinder with shear plate assembly have been assumed by trial-and-error method as; $k_2 = 50{,}000$ N/m, $k_3 = 50{,}000$ N/m, and $c_3 = 75{,}000$ N s/m.
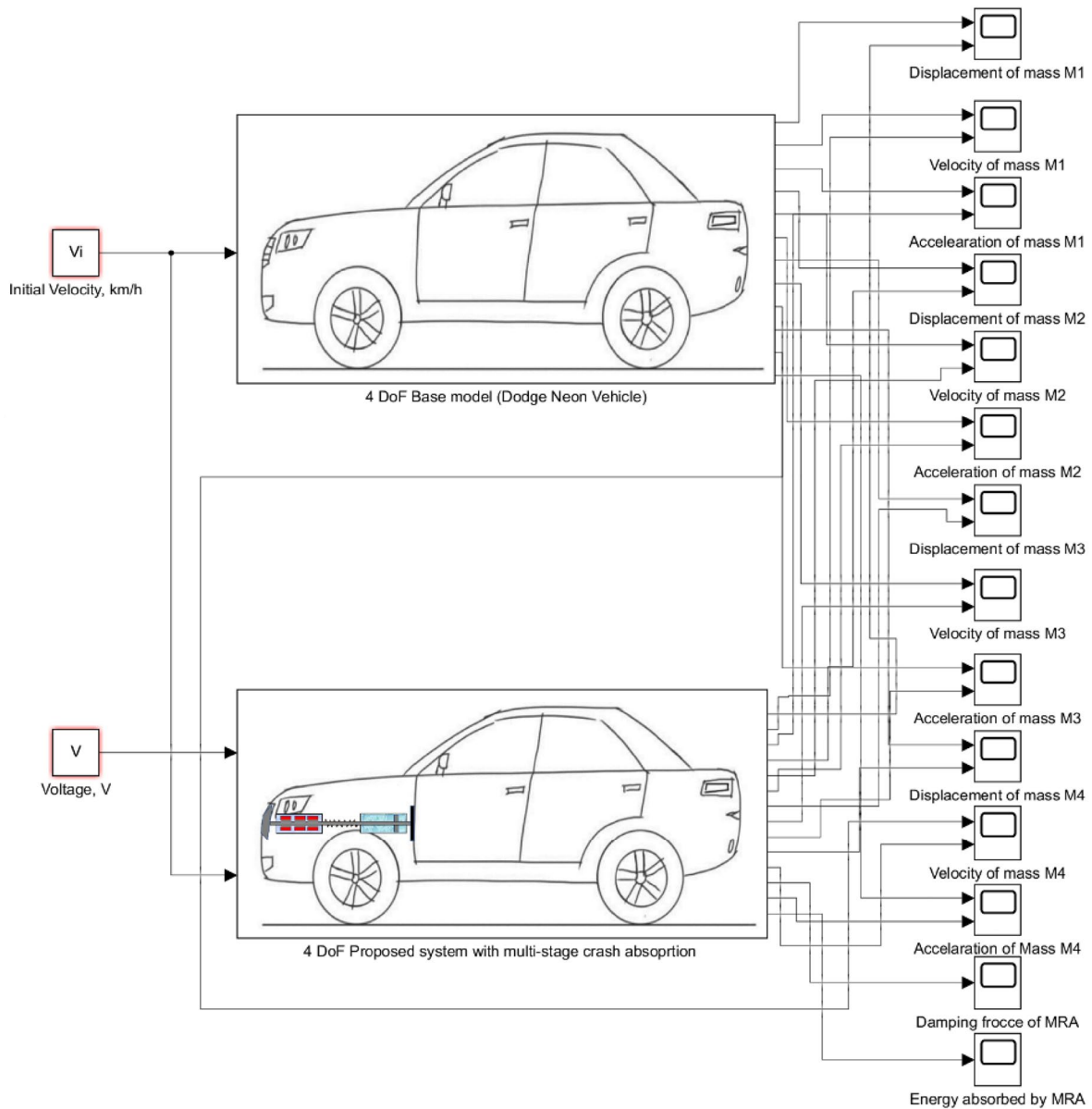

Fig. 10 Simulink model of base and proposed models

4 Dynamic simulation and results

The dynamic simulation has been performed in MAT-LAB SIMULINK platform. The inputs used in the simulation are V_i and V to the MRA, ranging from 35 to 85 km/h to address both low and high-speed crash phenomena and from 0 to 2.5 V for all simulation conditions respectively. Whereas, outputs considered for the system are crash kinematics of occupant's cabin (displacement, velocity, and acceleration) and parameters associated with MRA & other elements. The Simulink model of base and proposed models has been built and is depicted in Fig. 10.
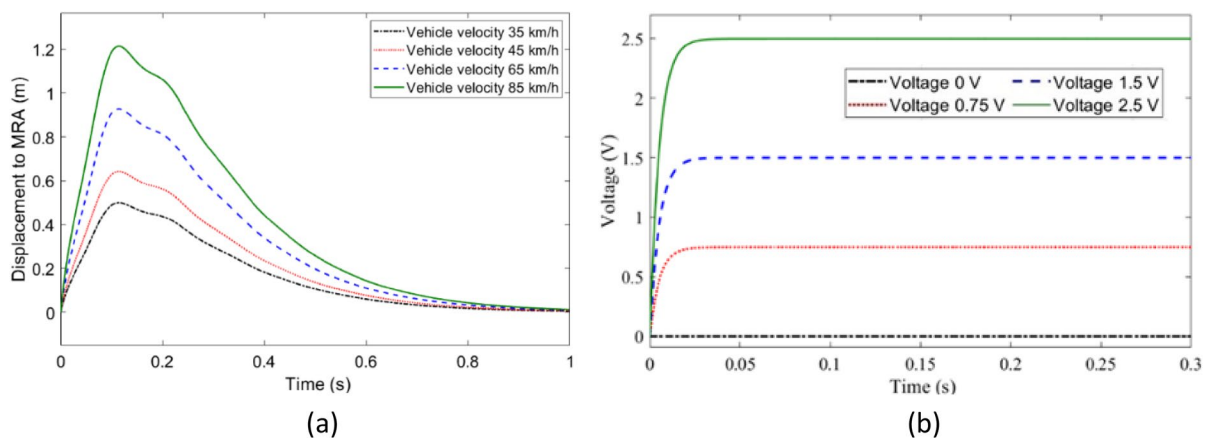
4.1 Crash kinematics

The impact of the vehicle is initially encountered by the bumper and after that it is transmitted to MRA. The MRA is positioned just beside M_2, thus the displacement of MRA is same as the displacement of M_2. The impact displacements of MRA for different impact speeds of the vehicle ranging from 35 to 85 km/h, have been extracted from the simulation and shown in Fig. 11a. This is further sent to the proposed model as an input variable. The damping force produced by MRA is altered by adjusting the field of electromagnetic coil by varying the voltage supplied to the coil in the range of 0–2.5 V, as depicted in Fig. 11b.

The crash kinematics of the lumped masses (various frontal mechanical and structural parts of the vehicle) are obtained from the numerical simulation
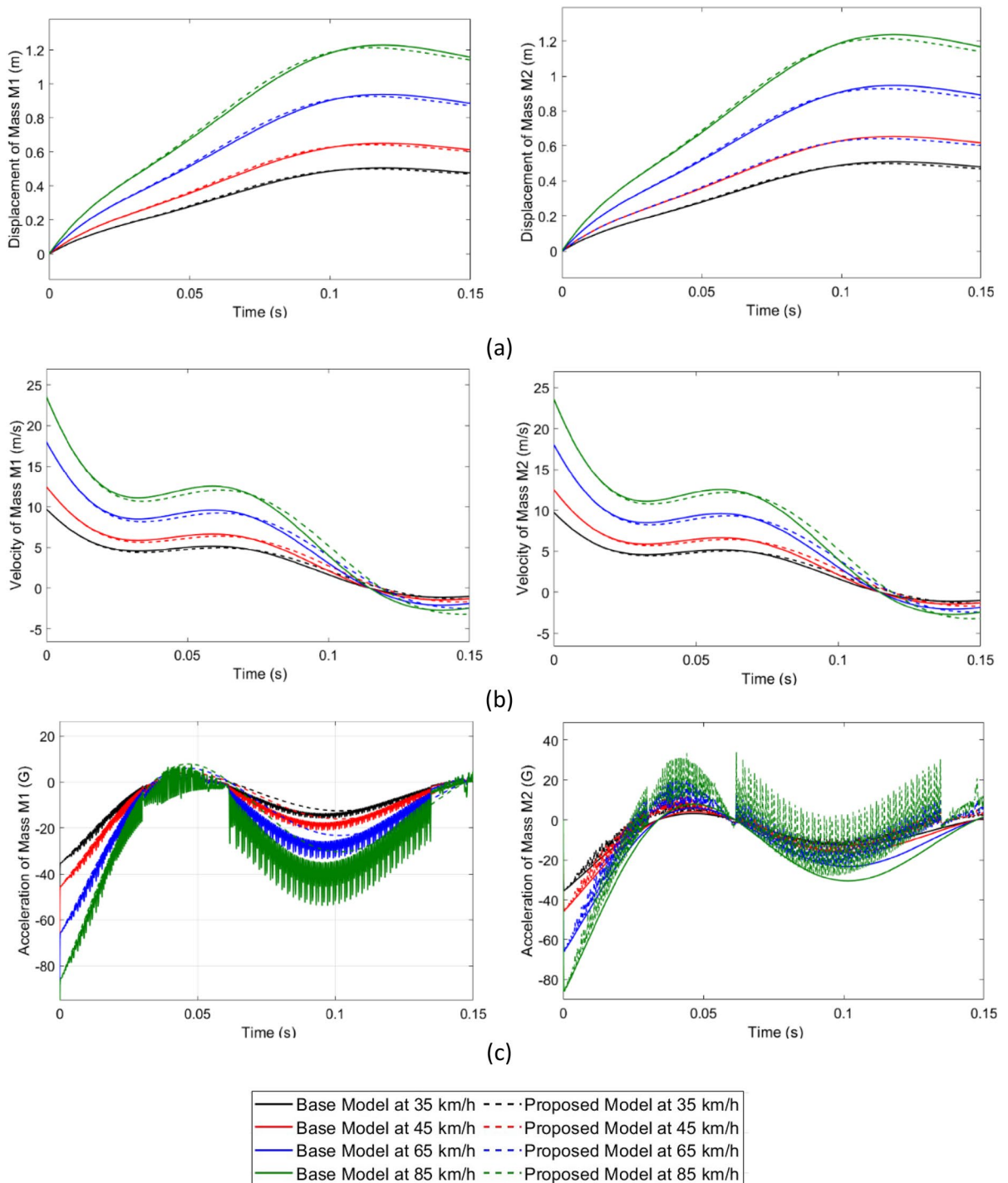
for both base and the proposed system. Figure 12 represents the kinematics of M_1 and M_2 for different speeds of the vehicle during a frontal impact with a stationary barrier. The displacement of the masses has been plotted with respect to time, as shown in Fig. 12a. There is a noticeable reduction of displacement of both the masses of the proposed model related with the base model. Subsequently, the velocity of the proposed model is reduced abruptly from the initial velocity to zero with higher settling time, as depicted in Fig. 12b for both M_1 and M_2. A noticeable decrement in the acceleration of masses is also observed compared with the base model for different speeds, as shown in Fig. 12c.

The crash kinematics of M_3 is shown in Fig. 13 which is mostly influenced by the performance of MRA. The displacement of M_3 is decreased from 0.5041 to 0.4937 m for 35 km/h and a similar reduction is obtained for various velocities, as shown in Fig. 13a. The velocity is also reduced drastically in a short period, as shown in Fig. 13b. The deceleration of the M_3 is depicted in Fig. 13c, which resembles that there is a reduction of 8.2% compared with the existing model.

The intrusion of the occupant's cabin of a car is shown in Fig. 14a, where in kinematics of M4 are considered. The proposed model has the least peak displacement than the base model for all initial velocities of the vehicle considered for the simulation. The velocity of the car is drastically reduced during the crash and the vehicle comes to rest within a short period. The proposed model has the capability

Fig. 11 Input parameters of MRA for various speeds of the vehicle, **a** Displacement of MRA after an impact and **b** applied voltage

(a)

(b)

(c)

Base Model at 35 km/h ---·Proposed Model at 35 km/h
Base Model at 45 km/h ---·Proposed Model at 45 km/h
Base Model at 65 km/h ---·Proposed Model at 65 km/h
Base Model at 85 km/h ---·Proposed Model at 85 km/h

Fig. 12 Comparison of crash kinematics of M_1 and M_2 of base and proposed models for various velocties of the vehicle, **a** Displacement, **b** Velocity, and **c** Acceleration
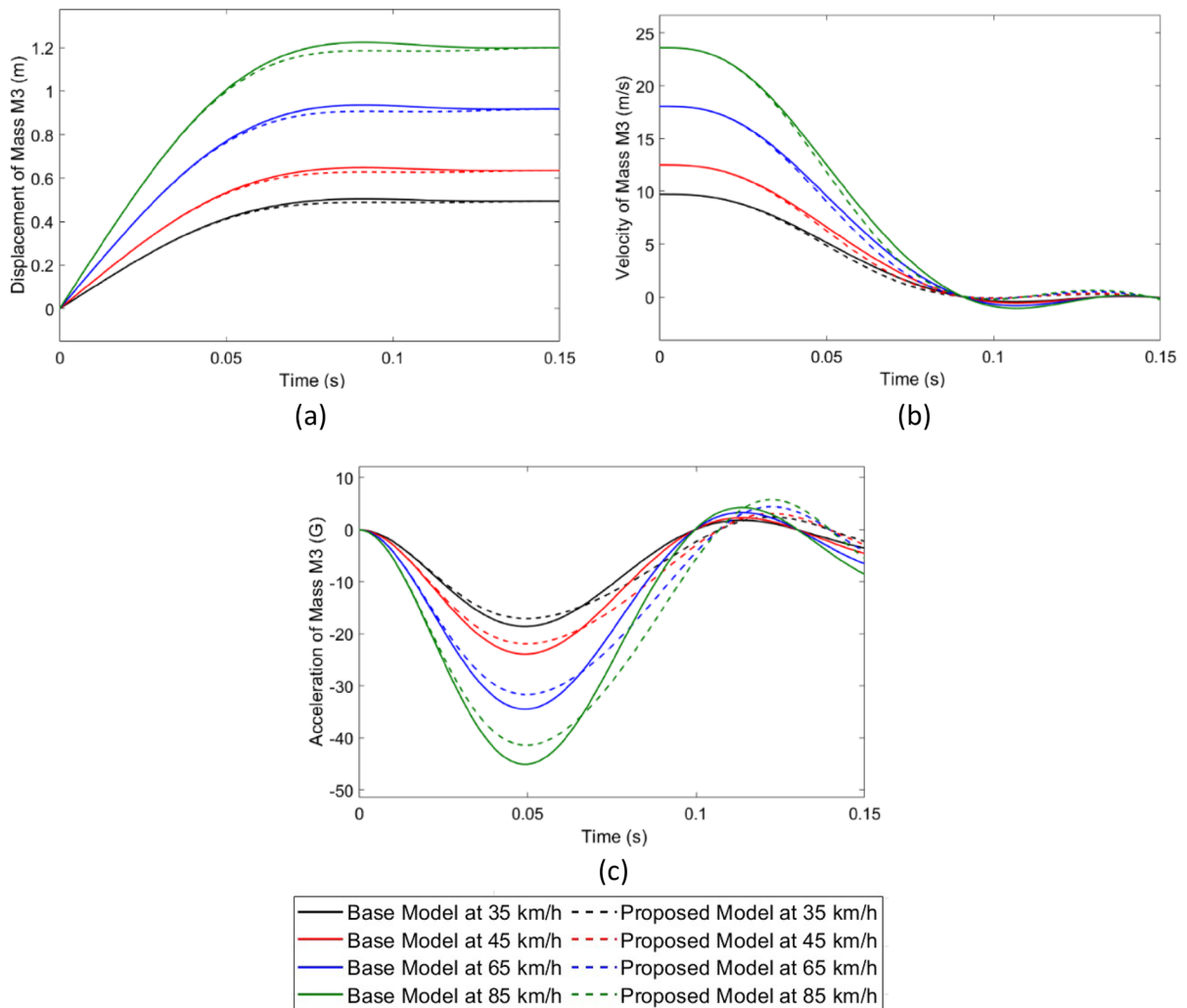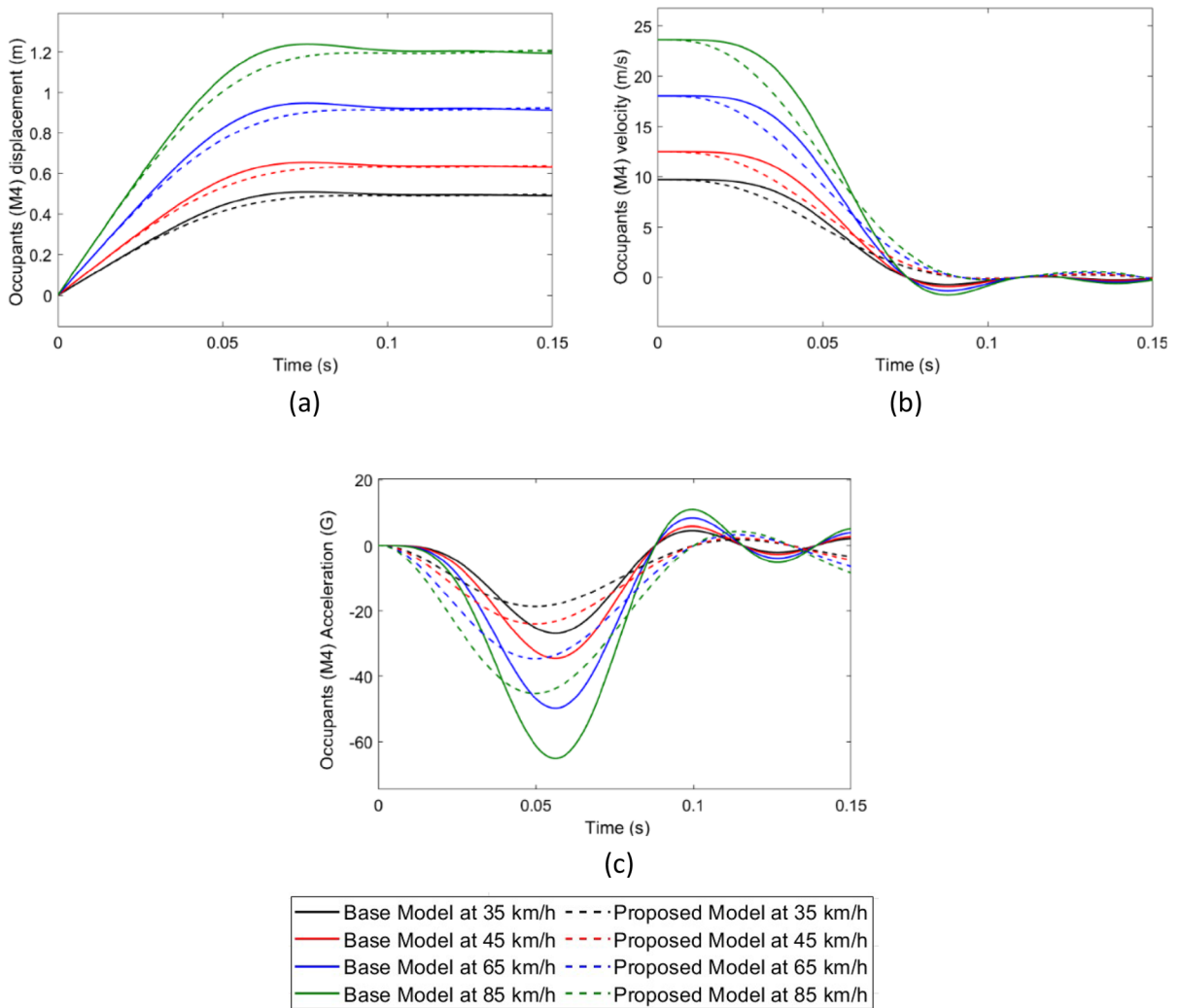
Fig. 13 Comparison of crash kinematics of M_3 of base and proposed models for different speeds of the vehicle, **a** Displacement, **b** Velocity, and **c** Acceleration

of increasing settling time, from 0.0756 to 0.1105 s, compared with the existing /base model, as depicted in Fig. 14b. The passenger safety mainly depends on the deceleration coming from restraint mechanism which is activated after an impact. The maximum acceleration of the proposed model has been decreased substantially, by almost 30.53%, for every impact velocity of the vehicle compared with base model, as seen in Fig. 14c. The comparison of peak displacement for both base and proposed system for each lumped mass is presented in Table 4. A substantial reduction of peak intrusion in each stage is

observed and finally the intrusion of the occupant's cabin gets reduced.

The peak displacement and deceleration of occupant's cabin (M_4) are presented in Table 5, for a clear understanding of the capability of the proposed model related with the existing model. Accordingly, the time of peak entity is also shown in Table 5 to justify the crashworthiness of the proposed model. The peak intrusion occurs at 0.076 s for the base model and for the proposed model it is 0.147 s. Certainly, the time for peak intrusion to occur is increased by 93.42% compared with the base model. While, the time of peak deceleration is reduced by 10.71%.

Fig. 14 Comparison of crash kinematics of occupant's cabin (M_4) for base and proposed models for different speeds of the vehicle, **a** Displacement, **b** Velocity, and **c** Acceleration

Table 4 Comparison of peak displacement of lumped masses for various speeds of the car

Velocity (km/h)	Maximum displacement (m)					
	Mass M_1		Mass M_2		Mass M_3	
	Base model	Proposed model	Base model	Proposed model	Base model	Proposed model
35	0.5056	0.4994	0.5940	0.4996	0.5041	0.4937
45	0.6500	0.6421	0.6550	0.6424	0.6481	0.6348
65	0.9389	0.9274	0.9461	0.9279	0.9362	0.9170
85	1.2280	1.2128	1.2370	1.2135	1.2240	1.1991

Table 5 Comparison between peak displacement, deceleration for various velocities of occupant's cabin (M_4) of the vehicle for base and proposed models

Model	Velocity (km/h)	Peak displacement (m)	T_{peak} (s)	Peak Deceleration (g)	T_{peak} (s)
Base model	35	0.5099	0.0760	26.80	0.0560
	45	0.6556	0.0760	34.45	0.0560
	65	0.9470	0.0760	49.76	0.0560
	85	1.2383	0.0760	65.08	0.0560
Proposed model	35	0.4969	0.1470	18.62	0.0500
	45	0.6389	0.1470	23.94	0.0500
	65	0.9228	0.1470	34.58	0.0500
	85	1.2068	0.1470	45.21	0.0500

4.2 Characteristics and behaviour of crash energy absorption elements other than MRA

The numerical analysis has been done for the estimation of forces encountered in each stage of the proposed four-stage crash absorption system for their behaviour during the crash for various impact speeds of the vehicle. A single series configuration of the proposed system has been considered for calculation of the forces and for capturing the behaviour of the energy absorption elements as well.

4.2.1 For bumper (stage-1)

The bumper is a crushable element, and it is an essential part of every vehicle, which generally reduces the transmission of impact force to the vehicle's passenger cabin during crash. A single series configuration with half of stiffness and damping coefficient of bumper in the proposed collision energy absorption system is considered for the analytical formulation of force (F_1) experienced by the bumper as under.

$$F_1 = \frac{1}{2}(c\dot{x}_1 + kx_1) \tag{18}$$

The simulation has been performed for different speeds of the vehicle to get insights into the behaviour of the bumper during crash. The numerical data has been plotted in Fig. 15. The bumper is an initial element that encounters the first impact when the vehicle is crashed with a stationary barrier, eventually receive higher impact force i.e., from 100.24 to 243.44 kN is absorbed or dissipated at stage-1 for various impact velocities, as shown in Fig. 15a. The displacement and force of M_1 are plotted in X and Y

axes respectively in Fig. 15b, which depicts a nonlinear pattern. The peak displacement of the proposed model varies between 0.4994 and 1.2128 m for different impact speeds. The force at each velocity is initially high and reduced drastically thereafter and finally becomes zero with dissipation of energy through intrusion/crushing of the frontal bumper. The force vs velocity plot (Fig. 15c) which exhibits almost a linear pattern for various impact velocities.

4.2.2 For spring (stage-3)

A spring with high stiffness has been used in stage-3 to encounter and establish further reduction in impact force that has been transmitted through MRA. The force has been calculated for all initial velocities of the vehicle by the following expression,

$$F_3 = k_2(x_3 - x_2) \tag{19}$$

The numerical data has been plotted to get the characteristics of spring, and is shown in Fig. 16. The maximum force at stage-3 is varying from 6.395 to 15.529 kN for different speeds of the vehicle, as shown in Fig. 16a. This force is exponentially decaying with 0.3 s. The displacement vs force relationship is shown in Fig. 16b, which depicts maximum displacement between 0.4937 and 1.1991 m and a curvilinear pattern is obtained for different speeds. Whereas, a half-circular pattern has been observed for velocity vs force at stage-3 which is shown in Fig. 16c. The reason for a such a pattern would be, vehicle's velocity gets reduced after an impact with an increase in the development of resistive force and finally reaches to rest due to the inertia.
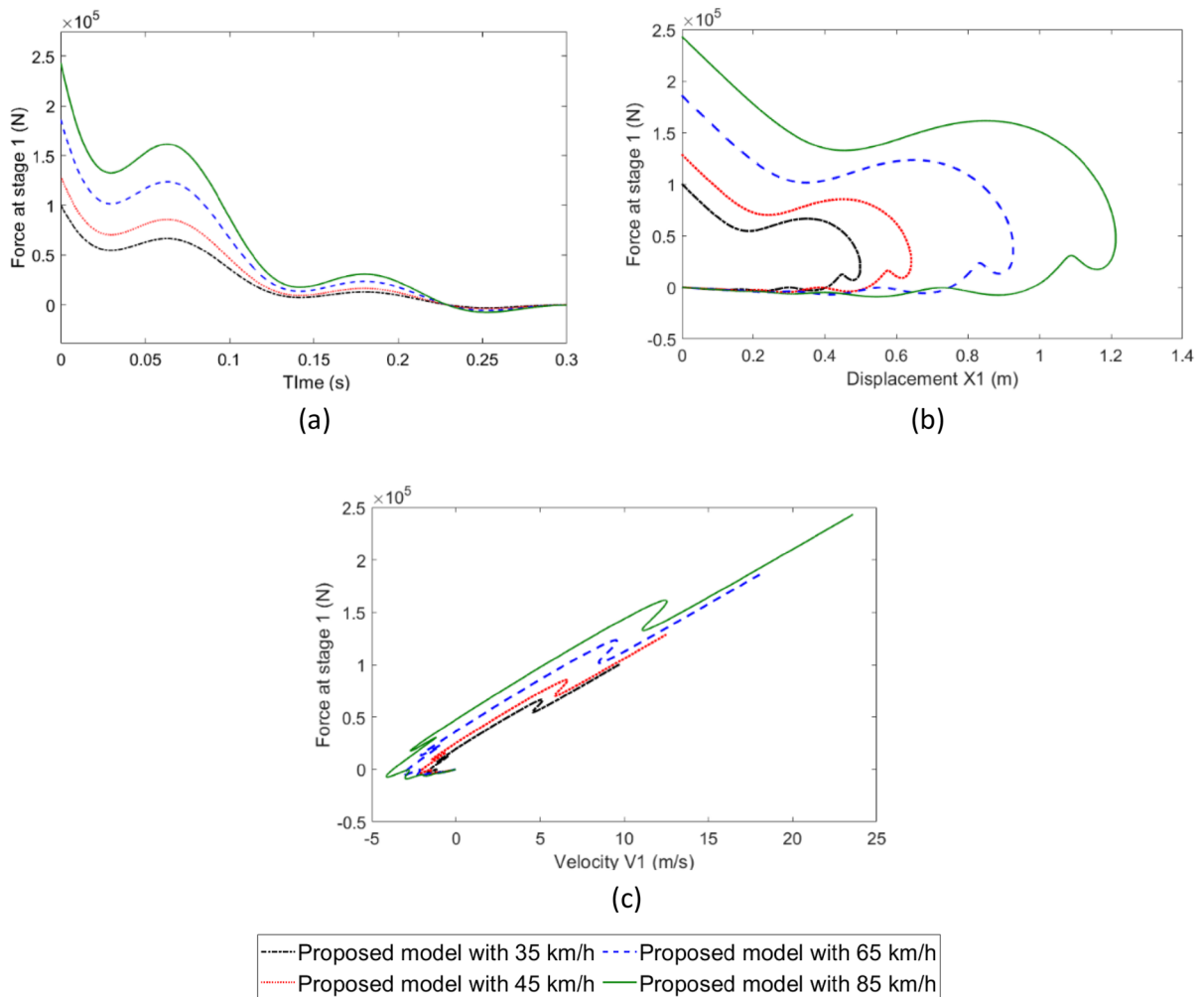
Fig. 15 Behaviour of bumper (stage-1) during crash for various speeds of the vehicle, **a** Force, **b** Force vs displacement, and **c** Force vs Velocity

### 4.2.3 For piston cylinder with shear plate assembly (stage-4)

The final stage is a piston-cylinder with shear plate assembly. The impact force, which is left after the passage of three stages is finally experienced by this assembly. The force acts in this stage is calculated based on the following expression,

$$F_4 = c_3(\dot{x}_4 - \dot{x}_3) + k_3(x_4 - x_3) \tag{20}$$

The peak forces experienced by this element are 6.540 kN and 15.882 kN for different speeds of the vehicle. Moreover, force is decaying exponentially

due to the underdamped state of the system as shown in Fig. 17a. A curvilinear pattern has been observed by plotting the datasets of displacement and force in cartesian plot, as shown in Fig. 17b. The maximum displacement is varying from 0.4969 to 1.2068 m. The velocity vs force relationship is depicted in Fig. 17c, which reveals a half circular pattern similar to force vs velocity response in stage 3.

The force experienced by each stage to counteract the impact force coming from the high-speed crash of the vehicle has been presented in Table 6. It is noticed that the bumper experiences high impact force because it is the stage-1 of the crash absorption system. After that, the intrusion displacement passes
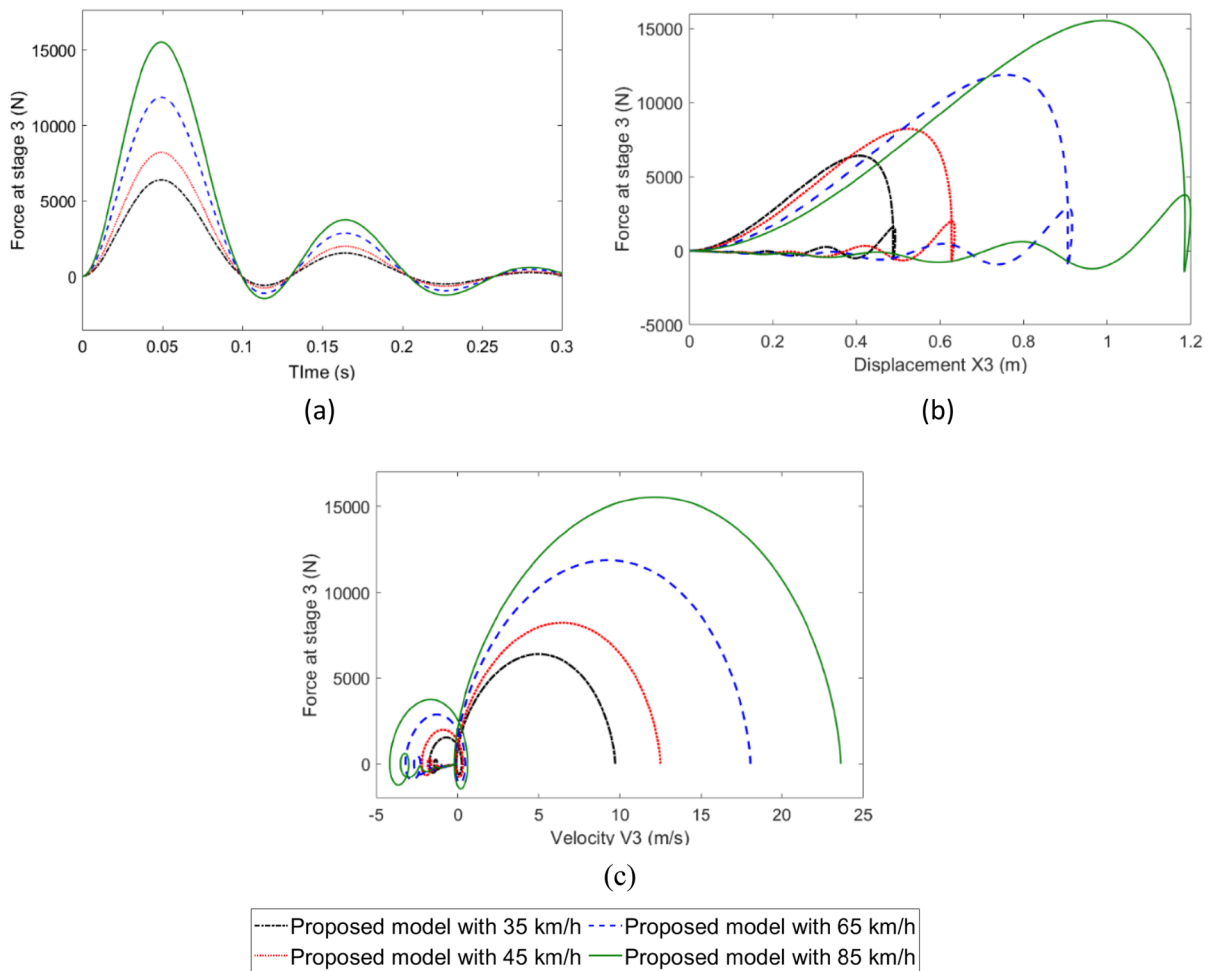
Fig. 16 Behaviour of spring (stage-3) during crash for different speeds of the vehicle. **a** Force, **b** Force vs displacement. **c** Force vs velocity

through the MRA stage and next to stage 3, and finally to stage-4. The last two stages absorbed less force compared to the other two because most of the impact force has been reduced in the frontal stages (first two) itself.

4.3 The characteristics and behaviour of MRA at Stage-2

The performance of MRA needs to be captured in terms of impact related circumstances to establish its capability while considering non-linear behaviour for low, medium, and high-speed vehicle crashes. This behaviour has been studied with fixed barrier for various initial velocities. Simultaneously,

the damping characteristics of the MRA is also investigated for various voltages applied externally.

The damping force and energy absorbed by MRA with various initial velocities of the automobile are depicted in Fig. 18a and b respectively. It has been observed that, higher the initial velocities of the vehicle, greater is the generated damping force and energy absorption by MRA. The maximum damping force and also peak energy absorption are varying from 62.10 to 148.6 kN and 22.06 to 129.0 kJ respectively for various impact speeds ranging from 35 to 85 km/h.

The characteristic plots such as displacement vs damping force and velocity vs damping force have also been plotted. Here, both displacement and
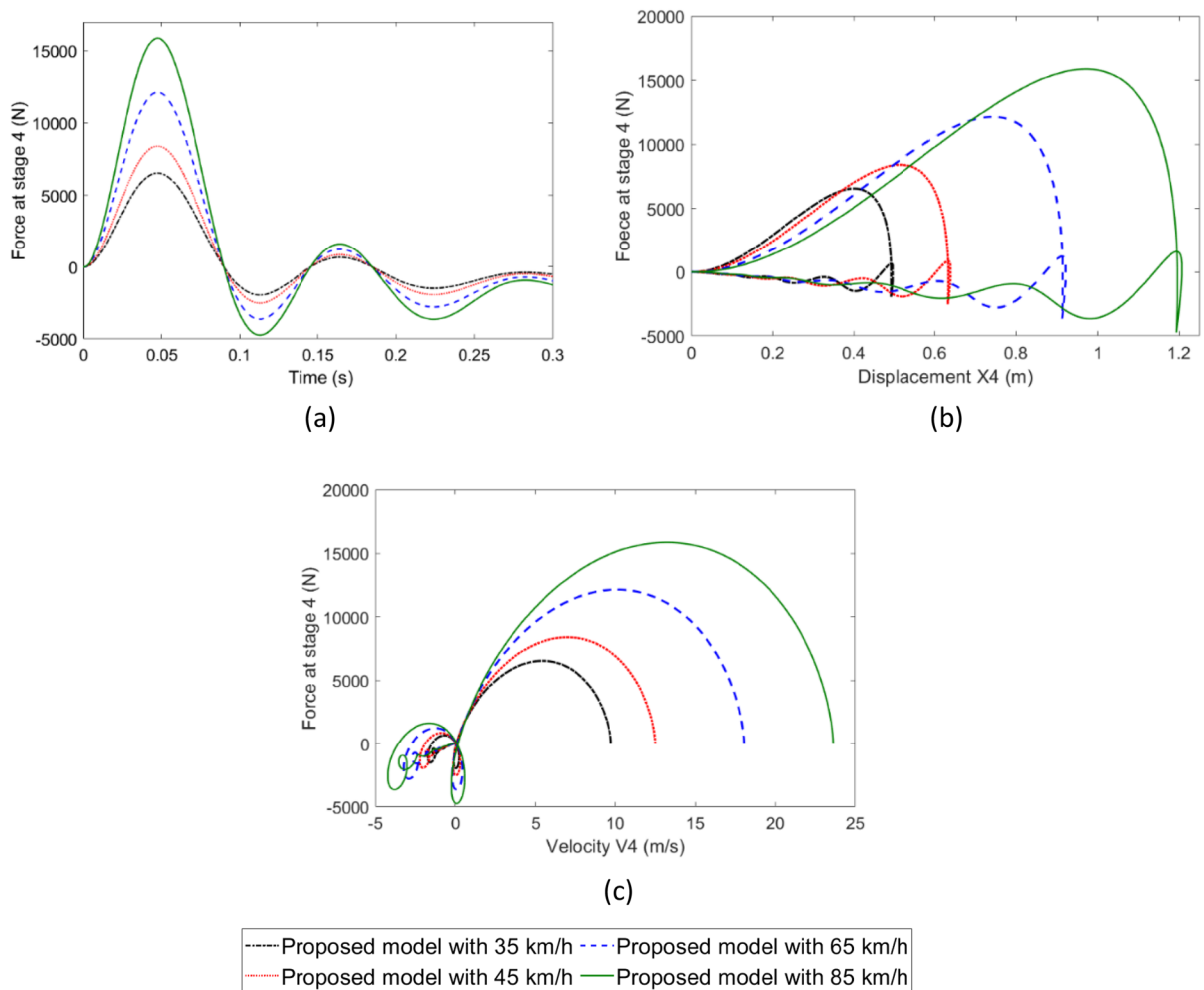
Fig. 17 Behaviour of piston cylinder with shear plate assembly (stage-4) during crash for various initial velocities of vehicle, **a** Force, **b** Force vs displacement, and **c** Force vs velocity

Table 6 Comparison of peak force experienced during different stages of the proposed system for various impact speeds of the vehicle

Force (kN)	Velocity of the vehicle, km/h			
	35	45	65	85
F_1	100.24	128.88	186.16	243.44
F_{MR}	62.28	79.93	114.81	149.09
F_3	6.39	8.22	11.88	15.53
F_4	6.54	8.41	12.15	15.88

velocity terms used are related to kinematics of MRA piston. It is observed that, displacement of MRA is only in the positive X-direction, and there is no displacement in the negative direction because the impact displacement which is fed to MRA is always positive. The pattern is similar for different speeds of the vehicle at constant 2.5 V and found that, the response looks like a conventional conch shell shape, as shown in Fig. 18c. The reason for such a pattern would be, the force developed by MRA during an impact increase with an increase in displacement reaches a maximum and gets reduced afterwards with a small increment in displacement and to end reaches the original position due to inertial effect. The peak displacement of the MRA is varying from 0.4996 to 1.2135 m and corresponding damping force is varying from 62.10 to 148.6 kN. The damping force vs velocity plot is shown in Fig. 18d and observed a
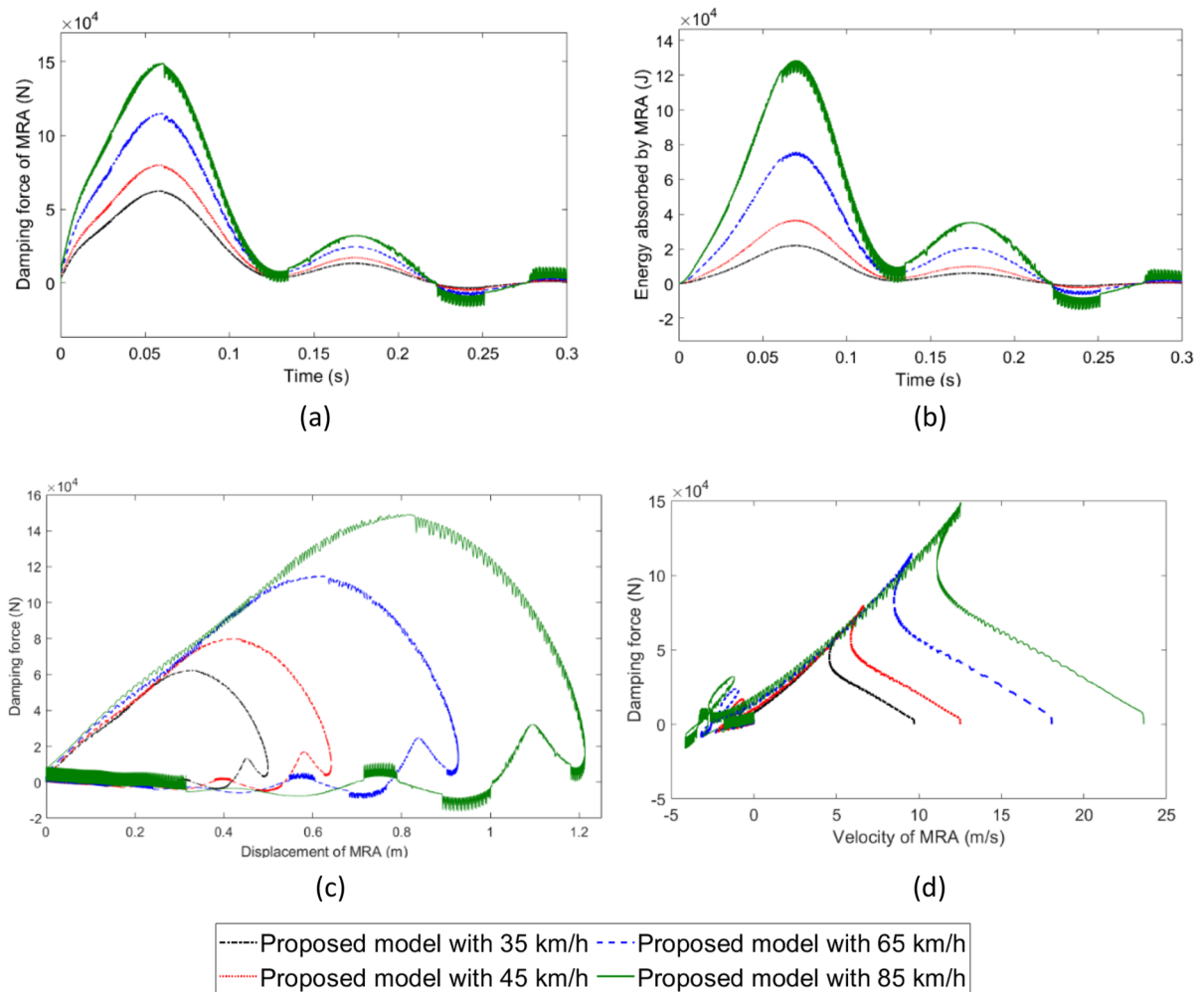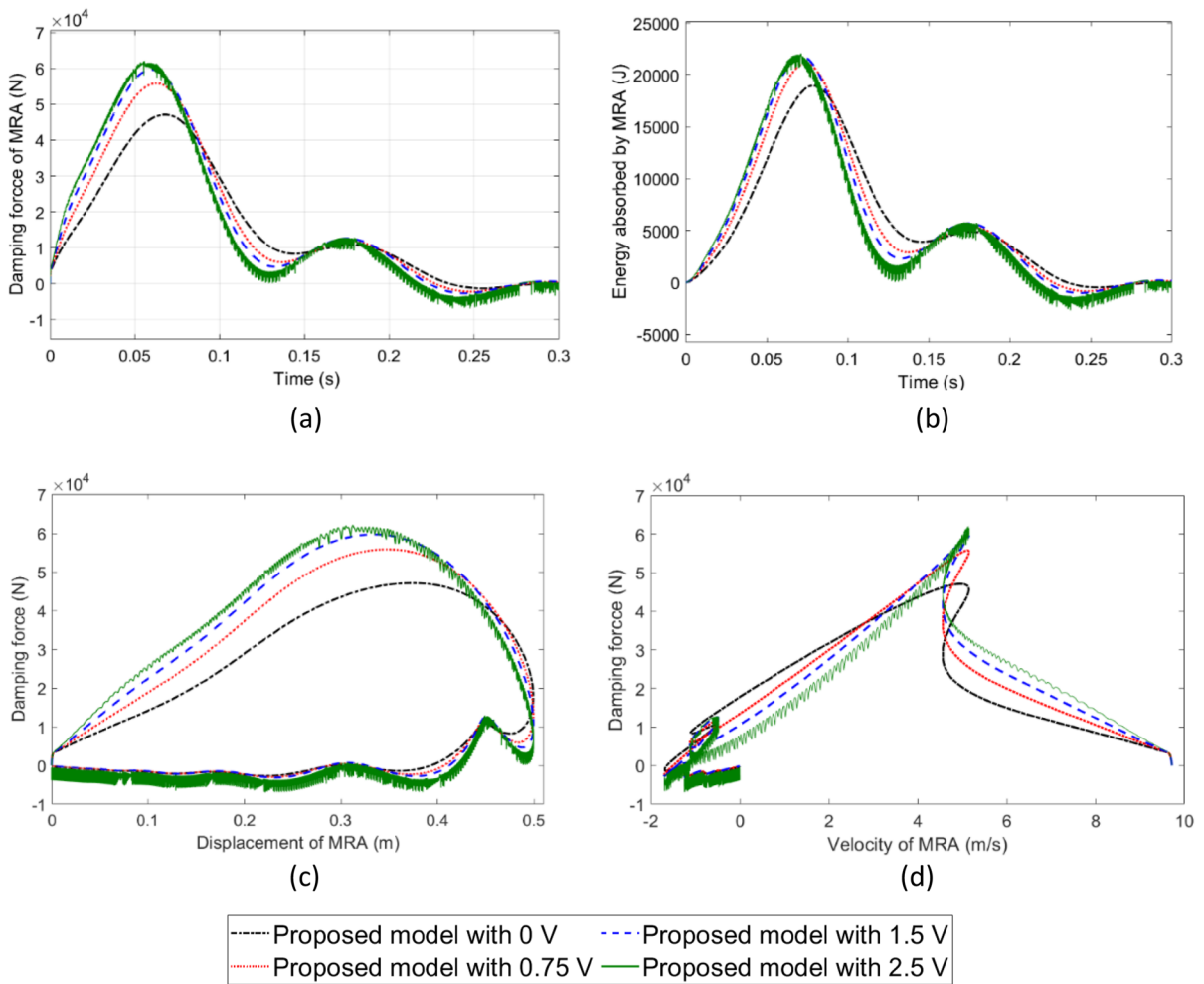
Fig. 18 Characteristics of MRA during crash for various speeds of vehicle at constant 2.5 V. **a** Damping force, **b** Energy absorbed, **c** Damping force vs displacement, and **d** Damping force vs velocity

non-linear pattern, which is almost similar for all velocities of the vehicle when there is a variation in the damping force.

The behaviour of vehicle when integrated with the proposed MRA assembly during crash for various voltages but at constant initial velocity of vehicle (35 km/h) is shown in Fig. 19. The damping force is increasing with increase of voltage and varies between 47.02 and 62.10 kN, as shown in Fig. 19a. The energy absorption capability of MRA for different voltages is also plotted to confirm on the capability of MRA during crash and is shown in Fig. 19b, which depicts that the maximum energy is varying from 18.95 to 22.06 kJ for 0–2.5 V applied.

The displacement of piston of MRA is plotted with damping force. The maximum displacement of MRA is found 0.4996 m at constant velocity of the vehicle and corresponding peak damping force is found to be varying from 47.02 and 62.10 kN respectively for various voltages as depicted in Fig. 19c. The response resembles like the conventional conch shell type of pattern similar to previous response of damping force vs displacement. The velocity response corresponding to generated damping force is shown in Fig. 19d, which follows a nonlinear pattern and similar pattern is observed for various voltages.

The damping force needs to be considered as a main attribute, as it predominantly adjusts the system

Fig. 19 Behaviour of MRA during crash for various voltages at a constant vehicle velocity of 35 km/h, **a** Damping force, **b** energy absorbed, **c** damping force vs displacement, and **d** damping force vs velocity

Table 7 Comparison of peak damping force of MRA for different impact speeds of the vehicle and voltage supplied to MRA

Voltage (V)	Velocity of the vehicle, km/h							
	35		45		65		85	
	F_{max} (kN)	T_{peak} (s)	F_{max} (kN)	T_{peak} (s)	F_{max} (kN)	T_{peak} (s)	F_{max} (kN)	T_{peak} (s)
0	47.020	0.068	58.290	0.068	75.350	0.068	85.150	0.064
0.75	55.770	0.063	70.870	0.063	98.620	0.064	121.200	0.064
1.5	59.690	0.060	76.380	0.060	108.700	0.061	138.700	0.061
2.5	62.100	0.056	79.770	0.056	114.600	0.056	148.600	0.057

during the crash. Thus, the damping force of MRA by varying both voltages supplied to MRA and impact speeds of the vehicle along with corresponding peak time are tabulated in Table 7. These results confirm that the damping force is proportional to both velocity

and voltages and varies between 47.02 to 148.6 kN dynamically. The time to attain maximum damping force is called as the peak time and is same for all velocities but varies for different voltages.

Table 8 Comparison of peak energy absorbed by MRA different impact speeds of the vehicle and voltage supplied to MRA

Voltage (V)	Velocity of the vehicle, km/h							
	35		45		65		85	
	E_{max} (kJ)	T_{peak} (s)	E_{max} (kJ)	T_{peak} (s)	E_{max} (kJ)	T_{peak} (s)	E_{max} (kJ)	T_{peak} (s)
0	18.950	0.079	30.510	0.079	58.350	0.081	87.270	0.084
0.75	21.100	0.074	34.660	0.074	70.710	0.075	115.900	0.076
1.5	21.800	0.071	35.960	0.072	74.500	0.072	125.800	0.072
2.5	22.060	0.071	36.250	0.073	75.930	0.068	129.000	0.071

The energy absorbed by MRA is an ultimate objective to counteract the intrusion of the vehicle during an impact with stationary barrier. Hence, the data has been gathered and is shown in Table 8 to understand the variation of the energy absorbed by MRA. It is observed that the energy is proportionately varying between 18.95 and 129.0 kJ for different speeds of the vehicle and also for different voltages. Finally, energy absorbed by MRA can calculated by considering the following standard expression (Archakam and Muthuswamy 2021),

$$E_{MR} = \int F_{MR}.d(x_{rel}) \qquad (21)$$

5 Conclusions

An attempt has been made to develop a four-stage crash energy absorption system with MRA as one of the energy absorbing elements. The proposed model consists of bumper, MRA, spring, and a piston cylinder with a shear plate assembly. This system was modelled with LPM by considering the Spencer model for MRA and spring-dashpot for other elements. The dynamic equations are derived for both base and the proposed models. The optimized parameters have been selected by considering a real-time crash test of Dodge Neon vehicle and for MRA, damper parameters related to 200 kN have been considered.

The dynamic model is simulated in MATLAB-SIMULINK. The comparison has been made between both the base and the proposed model to validate it in terms of crash kinematics and time of maximum entity. The output reveals that the proposed model exhibits the least peak displacement and peak deceleration of the occupant's cabin has been reduced by 30.53% compared with the base model. The time of peak displacement has been increased by 93.42% and the time of maximum deceleration has been reduced by 10.71% for the proposed model compared with the existing model. Accordingly, the behaviour of various embedded elements of the proposed system has been studied. Finally, the characteristics of MRA have been captured for different speeds of the vehicle and also for different voltages supplied to MRA to justify its capabilities in crash energy absorption.

The proposed model is complex due to multiple governing parameters and thus, the future study will be to develop a simplified control scheme. The optimized control attributes for both MRA and vehicle based on severity of the crash will also be studied.

References

Ahamed, R., Choi, S.B., Ferdaus, M.M.: A state of art on magneto-rheological materials and their potential applications. J. Intell. Mater. Syst. Struct. **29**, 2051–2095 (2018). https://doi.org/10.1177/1045389X18754350

Archakam, P.K., Muthuswamy, S.: Design and simulation of a crash energy absorption system integrated with magneto-rheological absorber. J. Vib. Eng. Technol. **9**, 1635–1656 (2021). https://doi.org/10.1007/s42417-021-00318-6

Azar, B.F., Veladi, H., Talatahari, S., Raeesi, F.: Optimal design of magnetorheological damper based on tuning

Bouc-Wen model parameters using hybrid algorithms. KSCE J. Civ. Eng. **24**, 867–878 (2020). https://doi.org/10.1007/s12205-020-0988-z

Bompos, D.A., Nikolakopoulos, P.G.: CFD simulation of magnetorheological fluid journal bearings. Simul. Model. Pract. Theory. **19**, 1035–1060 (2011). https://doi.org/10.1016/j.simpat.2011.01.001

Cao, L., Wang, H., Wu, J., Chen, H.: Study on a pneumatic automatic-extendable crash energy absorption system. Adv. Mater. Res. **455–456**, 1509–1514 (2012). https://doi.org/10.4028/www.scientific.net/AMR.455-456.1509

Elmarakbi, A.M., Zu, J.W.: Crash analysis and modeling of two vehicles in frontal collisions using two types of smart front-end structures: an analytical approach using IHBM. Int. J. Crashworthiness. **11**, 467–483 (2006). https://doi.org/10.1533/ijcr.2005.0117

Eshkabilov, S.: Modeling and simulation of non-linear and hysteresis behavior of magneto-rheological dampers in the example of quarter-car model. Commun. Control Sci. Eng. **4**, 12–29 (2016)

Gao, X., Niu, J., Liu, Z., Tian, J.: Semi-active control of ambulance stretcher system based on parallel mechanism with MR dampers and perturbation analysis. Int. J. Mech. Mater. Des. **15**, 817–831 (2019). https://doi.org/10.1007/s10999-019-09444-2

Goher, K.M., Chenhui, K., Fadlallah, S.O., Shabibi, A.M.A., Rawahi, N.Z.A.: Transient dynamic impact suppression of a Baja chassis using frontal and rear shock absorbers. Int. J. Crashworthiness. **22**, 676–688 (2017). https://doi.org/10.1080/13588265.2017.1301081

Hao, F., Lu, X., Qiao, Y., Chen, X.: Crashworthiness analysis of electric vehicle with energy-absorbing battery modules. J. Eng. Mater. Technol. Trans. ASME. (2017). https://doi.org/10.1115/1.4035498

Jain, S., Sreekumar, M.: The preliminary design of a collision energy absorption system. In: 6th International 27th All India Manufacturing Technologhy Design Research Conference, Pune, INDIA. 779–782 (2016)

Jawad, S.: Smart structures for frontal collision mitigation. SAE Tech. Pap. 1, (2002). https://doi.org/10.4271/2002-01-0247

Jiang, K., Wen, J.: Identification of nonlinear hysteretic systems using sequence model-based optimization. Struct Control Heal. Monit. **27**, 1–24 (2020). https://doi.org/10.1002/stc.2500

Kachhwaha, S.S., Singh, M.K., Sahu, D.P., Sahu, N.K.: Analysis of smart front-end structure in frontal crash mitigation. In: In: Deepak, B., Parhi, D., Jena, P. (eds) Innovative Product Design and Intelligent Manufacturing Systems. Lecture Notes in Mechanical Engineering. Springer, Singapore. pp. 631–639. Springer, Singapore (2020)

Khattab, A., & ElRahman, A.: Investigation of an adaptable crash energy management system to enhance vehicle crashworthiness (2010)

Krishna, H., Kumar, H., Gangadharan, K.: Optimization of magneto-rheological damper for maximizing magnetic flux density in the fluid flow gap through FEA and GA approaches. J. Inst. Eng. Ser. c. **98**, 533–539 (2017). https://doi.org/10.1007/s40032-016-0251-z

Liu, X., Gao, X., Yu, H., Ye, D.: Dynamic performance of different metal foam magnetorheological fluid materials. IEEE Trans. Magn. **51**, 1–5 (2015). https://doi.org/10.1109/TMAG.2015.2450682

Liu, G., Gao, F., Wang, D., Liao, W.-H.: Medical applications of magnetorheological fluid: a systematic review. Smart Mater. Struct. **31**, 043002 (2022). https://doi.org/10.1088/1361-665X/AC54E7

Marzbanrad, J., Pahlavani, M.: Calculation of vehicle-lumped model parameters considering occupant deceleration in frontal crash. Int. J. Crashworthiness. **16**, 439–455 (2011). https://doi.org/10.1080/13588265.2011.606995

Mei, L., Thole, C.A.: Data analysis for parallel car-crash simulation results and model optimization. Simul. Model. Pract. Theory. **16**, 329–337 (2008). https://doi.org/10.1016/j.simpat.2007.11.018

Muthalif, A.G.A., Razali, M.K.M., Nordin, N.H.D., Hamid, S.B.A.: Parametric estimation from empirical data using particle swarm optimization method for different magnetorheological damper models. IEEE Access. **9**, 72602–72613 (2021). https://doi.org/10.1109/ACCESS.2021.3080432

http://www.natrip.in/: National Automotive Testing and R&D Infrastructure Project (NATRiP), http://www.natrip.in/

Oh, J.S., Sohn, J.W., Choi, S.B.: Applications of magnetorheological fluid actuator to multi-DOF systems: state-of-the-art from 2015 to 2021. Actuators. **11**, 1–25 (2022). https://doi.org/10.3390/act11020044

Pisetskiy, S., Kermani, M.: High-performance magneto-rheological clutches for direct-drive actuation: design and development. J. Intell. Mater. Syst. Struct. **32**, 2582–2600 (2021). https://doi.org/10.1177/1045389X211006902

Rabinow, J.: The magnetic fluid clutch. Trans. Am. Inst. Electr. Eng. **67**, 1308–1315 (1948). https://doi.org/10.1109/T-AIEE.1948.5059821

Rossi, A., Orsini, F., Scorza, A., Botta, F., Belfiore, N.P., Sciuto, S.A.: A review on parametric dynamic models of magnetorheological dampers and their characterization methods. Actuators. (2018). https://doi.org/10.3390/act7020016

Spencer, B.F., Dyke, S.J., Sain, M.K., Carlson, J.D.: Phenomenological model for magnetorheological dampers. J. Eng. Mech. **123**, 230–238 (1997). https://doi.org/10.1061/(ASCE)0733-9399(1997)123:3(230)

Spencer, B.F., Yang, G., Carlson, J.D., Sain, M.K.: Smart dampers for seismic protection of structures : A full-scale study. In: Proceedings of the 2nd World Conference on Structural Control. pp. 1–10 (1998)

Suvarna, N., Raju, A., Hegde, S.: A review of magneto rheological fluid in suspension and torsional devices. AIP Conf. Proc. (2021). https://doi.org/10.1063/5.0036249

Talatahari, S., Kaveh, A., Mohajer Rahbari, N.: Parameter identification of Bouc-Wen model for MR fluid dampers using adaptive charged system search optimization. J. Mech. Sci. Technol. **26**, 2523–2534 (2012). https://doi.org/10.1007/s12206-012-0625-y

Xiao, Y., Yin, H., Fang, H., Wen, G.: Crashworthiness design of horsetail-bionic thin-walled structures under axial dynamic loading. Int. J. Mech. Mater. Des. **12**, 563–576 (2016). https://doi.org/10.1007/s10999-016-9341-6

Yuan, X., Tian, T., Ling, H., Qiu, T., He, H.: A review on structural development of magnetorheological fluid damper.

Shock Vib. **2019**, 1–33 (2019). https://doi.org/10.1155/2019/1498962

Zhi Shen, W., Hong Bo, W., Tiantian, G., Xu Hui, L.: Parameter optimization of a metal foam magneto-rheological damper. Int. J. Mech. Mater. Des. **16**, 323–330 (2020). https://doi.org/10.1007/s10999-019-09463-z

Zhu, X., Jing, X., Cheng, L.: Magnetorheological fluid dampers: A review on structure design and analysis. J. Intell. Mater. Syst. Struct. **23**, 839–873 (2012). https://doi.org/10.1177/1045389X12436735